ACS OMEGA

Open Access

http://pubs.acs.org/journal/acsodf

Article

Template-Free Synthesis of Phosphorus/Nitrogen-Doped Mesoporous Titania Materials with Excellent Adsorption for Lysozymes

Yajing Wang,* Xu Zhang, Peng Liu, Zhao Liu, Tiezhen Ren,* and Ziqian Wang

Cite This: *ACS Omega* 2023, 8, 49129−49136

Read Online

ACCESS | Metrics & More | Article Recommendations

ABSTRACT: Element-doped mesoporous titanium oxide has significant advantages in substance separation and adsorption due to its larger specific surface area and stronger hydrophobicity. However, its current synthesis methods have limitations such as complicated preparation process, high production cost, or not being environmentally friendly, and the synthesis of elementally doped titanium oxide materials by simple, low-cost, and green means is the research goal of this study. In this study, phosphorus-doped mesoporous titanium oxides (TiP) materials have been synthesized through a facile template-free method in an ethanol system, which were further modified by nitrogen doping with the use of urea as the nitrogen source. Both the synthesized TiP and P−N codoped sample (N-TiP) are amorphous with mesopores. It was revealed by FTIR and XPS spectra that the formation of Ti−O−P and −O−Ti−N bonds in the synthesized samples was due to the partial substitution of phosphorus for titanium in Ti−O−Ti bonds in mesoporous titanium oxide, while nitrogen replaced some oxygen in the −O−Ti−O bonds in the form of anions. The TiP sample was estimated by the BET method to have a relatively large surface area, up to 317 m^2/g. The adsorption of TiP and N-TiP materials to lysozyme protein in a buffer solution at different pH values showed that the adsorption of TiP to lysozyme protein was larger, which was 32.68 μmol/g. It shows that TiP has potential as a multifunctional adsorbent.

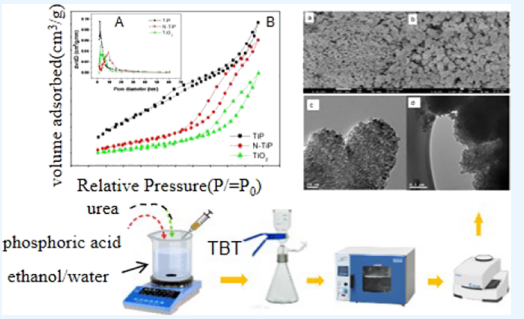

1. INTRODUCTION

TiO_2 is a typical N-type semiconductor oxide that has significant photocatalytic advantages. In order to improve the photon utilization and carrier separation efficiency of TiO_2-based photocatalysts, a lot of research has been carried out by using morphology control, doping, and heterostructure construction methods. Among them, nitrogen, carbon, sulfur, phosphorus, and other nonmetallic elements doping has become one of the most effective ways to improve the photocatalytic efficiency of TiO_2. Whereas, there are relatively few studies on the adsorption separation of nonelement doped TiO_2. In fact, ordered mesoporous titania shows specific selective adsorption performance and high adsorption capacity due to its large specific surface area, uniform pore structure, adjustable aperture, and relatively narrow pore size distribution.[1−5] Therefore, It is potential for mesoporous titania to be an ideal adsorption material since a variety of substances can assemble in its channel to separate biological macromolecules, organic small molecules, and heavy metal ions.[6−10] Belessi[11] reported the color of reactive brilliant red 195 could be removed significantly in pH = 3 by TiO_2 nanoparticles. However, the preparation of mesoporous titanium oxide materials is a strict and complicated synthesis process. Moreover, the surface functional groups are not enough to enhance the adsorption capability. Thus, it is very necessary to modify mesoporous TiO_2. One of the most effective methods is to doping elements on the surface of inorganic nanoparticles to form a modification layer. In this way, the stability of nanoparticles is enhanced, the agglomeration between nanoparticles is significantly reduced, and their ability to absorb organic compounds and metal ions is improved.[12−17]

A series of modified TiO_2 doped with different elements has very recently been reported as important adsorbents for the adsorption of pollutants. Feng[13] reported carbon-doped mesoporous titanium oxide materials had very high adsorption efficiency for the dye crystal violet. Zhang and Yun[16] reported the doping of Br was in favor of forming a rod-shaped network porous structure and improving the TiO_2 surface charge state, with the adsorption efficiency of cation blue X-GRL onto the surface of Br-doped nanoporous TiO_2 (Br/TiO_2) being up to 92.2%. Xiong et al.[18] demonstrated that Amorphous titanium

Received: September 20, 2023
Revised: November 24, 2023
Accepted: November 28, 2023
Published: December 13, 2023

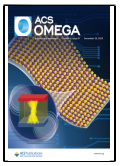

phosphates (ATP) doped with NH_4^+, K^+, Na^+, and Li^+ ions did not change the crystal form of ATP. Moreover, ATP-NH_4 has a saturated adsorption capacity for U(VI) as high as 505.1 mg g^{-1}, which may be an effective adsorbent to remove U(VI).

Adjusting the aperture size of mesoporous materials or modifying them with an organic functional group could be conducive to selectively adsorbing biological macromolecules such as specific proteins, RNA, and polysaccharides.[19] For instance, adsorption of lysozyme (Lz) was achieved on the nanofiber membrane,[20,21] Fe/CMK-5 Composites,[22] nanoporous carbon molecular sieves,[23] and hierarchical meso-macroporous aluminum phosphonate hybrid materials.[24] Lysozyme is an alkaline protein with stable chemical properties. Its antibacterial protection mechanism is significant. So far, lysozyme has been widely used in medicine, food, scientific research, and various industrial fields.[25] However, adsorptions of biological macromolecules on modified mesoporous TiO_2 doping by elements were rarely reported.

In general, many mesoporous phosphorus-doped titanium materials with a high specific surface area have been synthesized by template method using anionic surfactants, cationic surfactants, alkyl ammonium, and block copolymers as structure guiding agents.[26−29] However, mesoporous titanium phosphate prepared by the template method, in reality, has the potential for the transformation of the crystal and the collapse of the skeleton, thus the crystal structure was liable to be destroyed[30−34] due to the high temperature in the removement process of template agent. In addition, the template agent is very difficult to remove completely, thus reducing the mesoporous specific surface area. In order to further improve the physical, chemical, and technical properties of titanium phosphate adsorbents, it is important to synthesize template-free mesoporous titanium oxide doped with various elements by a simple and environmentally friendly synthesis method. In this work, syntheses of phosphorus-doped titanium oxide (TiP) and phosphorus−nitrogen codoped mesoporous titanium oxide (NTiP) were carried out through a facile template-free and one-step hydrothermal method in an ethanol system, at ambient temperature. The synthesized doped mesoporous Titania exhibited excellent adsorption capacity for biological macromolecule lysozyme by controlling the hydrolysis of tetrabutyl titanate and the assembly process of nanoparticle aggregation.

2. EXPERIMENTAL SECTION

2.1. Preparation of the Adsorbent. All of the purchased chemicals were used without further purification. The synthesis of the adsorbent was carried out without a template. The 2.3 g of phosphoric acid (98%) was dissolved in 37 mL of ethanol/water (30:1) solution, followed by the addition of 15 mL of urea (0.5 mol/L) solution. In order to promote the newly generated titanium alkoxide hydrolyze completely, 6.8 g of titanium(IV) butoxide (TBT) was then added drop by drop to the above solution and vigorously stirred at ambient temperature. The approximate molar ratio of Ti/P/ethanol/water in the mixture is 1:1:30:1. After stirring the mixture for 2 h, the product was filtered, washed with distilled water, dried at 80 °C for 12 h and then calcined at 500 °C for 3 h, which was marked as N-TiP. The synthesis was performed in the absence of urea, and the obtained solid was denoted as TiP. For comparison, pure TiO_2 was also prepared by hydrolyzation of titanium(IV) butoxide (TBT) in ethanol/water solution without phosphoric acid.

2.2. Characterization. X-ray diffraction (XRD) patterns were recorded on a Rigaku D/Max-2500 diffractometer using Cu K radiation operated at 40 kV and 100 mA. N_2 adsorption−desorption analysis was performed on a Quanta chrome NOVA 2000e sorption analyzer at a liquid nitrogen temperature (77 K). The sample was degassed at 200 °C overnight prior to the measurement. The surface area was obtained by the Brunauer−Emmett−Teller (BET) method, and the pore size distribution was calculated from the adsorption branch of the isotherm by the DFT model.

Scanning electron microscopy (SEM) was performed on a Jeol-JSM-6700F microscope at 20 keV. Transmission electron microscopy (TEM) was carried out on a Philips Tecnai G20 microscope, working at 200 kV. A trace amount of the sample was dispersed in an ethanol solution by sonication for 10 min and then deposited on a carbon-coated copper grid, which was used as a TEM specimen. The FTIR spectra of all samples were recorded on a Bruker Vector 22 spectrometer, with the KBr tablet technique. XPS measurements were performed with a Kratos Axis Ultra DLD spectrometer employing a monochromatic Al−Kα X-ray source (h = 1486.6 eV). UV−vis diffuse reflectance spectra of as-prepared samples were recorded on a TU-1901 spectrophotometer over the wavelength range of 190−900 nm with $BaSO_4$ used as the reference sample.

2.3. Lysozyme Adsorption Test. The lysozyme (Lz) adsorption was carried out as described in the literature.[21,22] A series of standard lysozyme (Lz) solutions with concentrations ranging from 20 to 280 μmol/L were prepared by dissolving different amounts of lysozyme (Lz) in 25 mmol/L buffer solutions (pH 6.5 potassium phosphate buffers, pH 9.6, 11and 12 sodium bicarbonate buffer). In each adsorption experiment, 50 mg of the adsorbent samples was suspended in 10 mL of the respective lysozyme solution and the fierce stirring was kept for 24h. The amount of lysozyme adsorbed was monitored by measuring the UV absorption at λ_{max} = 281.5 nm of the initial and final solutions. Centrifugation prior to analysis was necessary to avoid potential interference from suspended particles in the UV−vis analysis. The adsorption of lysozyme (Lz) was recorded at pH = 6.5, 9.6, 11 and 12, respectively. The isotherms for lysozyme (Lz) adsorption are of type L (Langmuir isotherm), and the monolayer capacities were calculated using the Langmuir equation. The comparison of the maximum amount adsorbed of lysozyme (Lz) was achieved at various pH values.

3. RESULTS AND DISCUSSION

3.1. Characterization of the Synthesized Materials. The microstructures of the synthesized samples were characterized by scanning electron microscopy. Figure 1a shows the representative SEM image of the TiP material, revealing that the irregular spherical particles are in the hundreds of nanometer scale. The samples N-TiP in Figure 1b composed of irregular nanoparticle aggregation have the same morphology, but the particle size is slightly enlarged, indicating that the macrostructure is retained and the appearance has not changed after urea solution is added in the system for nitridation. TEM images of the synthesized samples are shown in Figure 1c,d. It is seen that the nanoparticle of TiP is formed with a wormhole-like framework during alcohol−hydrolysis of TBT with the interspace of 2 nm (Figure 1c). Compared with TiP, the sample N-TiP, codoped by nitrogen and phosphorus, is also aggregated nanoparticles, while it has a vermiculate pore

https://doi.org/10.1021/acsomega.3c07222
ACS Omega 2023, 8, 49129−49136

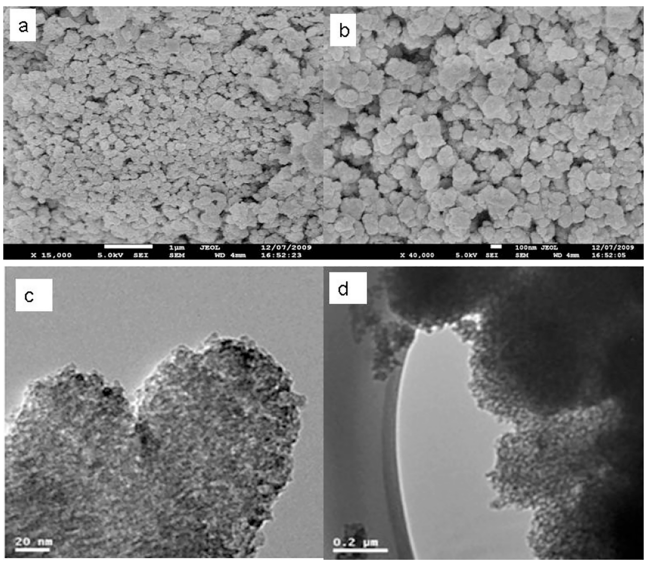

Figure 1. SEM images of (a) TiP and (b) N-TiP. TEM images of TiP (c) and N-TiP (d).

structure with a pore diameter of about 10 nm (Figure 1d). These observations suggest that the addition of urea has an effect on the water heating system, but it is not useful for the preparation of the nanoparticles.

The N_2 adsorption−desorption isotherms and corresponding pore size distribution (PSD) curves with the DFT model are shown in Figure 2. It is noticeable that the isotherms of TiP

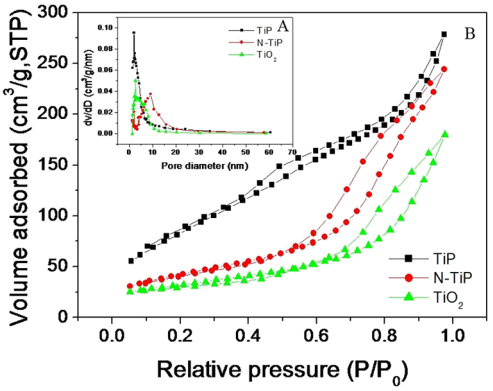

Figure 2. N_2 adsorption−desorption isotherms (A) and pore size distribution curves (B) of TiP, N-TiP, and TiO_2 with the DFT model.

are typical type IV with a hysteresis loop, indicating substantial textural mesoporosity with narrow slitlike pores are formed by aggregation (loose assembly) of platelike nanoparticles, while the hysteresis loop of TiP is type H3 because a steady trend of isotherms did not be observed when relative pressure was saturated. However, a strong uptake of the nitrogen-adsorbed volume is observed at a relative pressure greater than 0.85, which could suggest an appreciable amount of macropores (interparticle voids). The BET surface area of TiP is 317 m^2/g with an average pore size of 3.3 nm (Table 1), while the pore size of the N-TiP and TiO_2 is around 5.4 and 4.2 nm, respectively. The latter two samples (N-TiP and TiO_2) have a low surface area with isotherm of type II, indicating some textural macroporosity with only weak contribution of mesopores. Considering the decreased surface area, it is

Table 1. Summary of the Physicochemical Properties and Lysozyme Adsorption of the Synthesized Samples

sample	S_{BET} [a] m^2/g	D_{DFT} [b] nm	V_{pore} [c] cc/g	n_m [d] mg/g
TiP	317	3.3	0.464	470
N-TiP	153	5.4	0.384	374
TiO_2	113	4.2	0.271	301

[a]BET surface area calculated from the linear part of the 10-point BET plot. [b]Pore diameters estimated using the adsorption branch of the isotherm by the DFT method. [c]Single point total pore volume of pores at $P_0/P = 0.97$. [d]Monolayer adsorption capacities of adsorbents for lysozyme.

believed that urea has some effect on the polar end of the surfactant during the formation of micelles as described in the previous report.[34,35] In addition, it can be found from the average pore size distribution curves (Figure 2) that the aperture of the material is relatively wide, because the ester exchange reaction may produce between ethanol and titanium source TBT, then N-butyl alcohols generated in the reaction may participate in the self-assembly process, resulting in the mesoporous structure of different aperture size.

Figure 3 shows the XRD patterns of the prepared TiP and N-TiP samples together with that of pure TiO_2. The pure

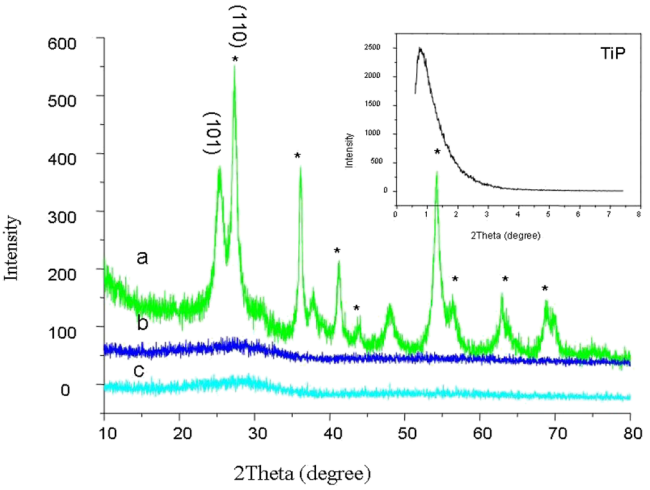

Figure 3. X-ray diffraction patterns of TiO_2 (a), TiP (b), and N-TiP (c). (Inset) small angle diffraction pattern of (b). * is for the rutile phase and the rest is for the anatase phase.

titania presents bicrystalline phases of anatase and rutile, while TiP and N-TiP have amorphous framework due to the broad peak of both the materials in the range of 15−40°. Sarkar et al.[36] synthesized titanium phosphate with a semicrystalline phase in assistance of hydrothermal treatment at 140 °C for 2 days. Compared with our synthesis route, the formation of the crystal phase had already been up to the aged temperature. Moreover, it is seen from small-angle X-ray diffraction patterns (inset) of TiP that one peak at around 0.7° (ca. 11 nm) indicates that the pore wall is very thick as well as the existence of nonordered mesopores. However, the low angle peak in samples N-TiP and TiO_2 is not observed, which might be ascribed to the aggregation form and the change of protocol during the preparation.

FTIR was performed to find out bond information on the structure, as shown in Figure 4A. The broadband at 3400 cm^{-1} and the band at 1630 cm^{-1} can mainly be attributed to the

https://doi.org/10.1021/acsomega.3c07222
ACS Omega 2023, 8, 49129−49136

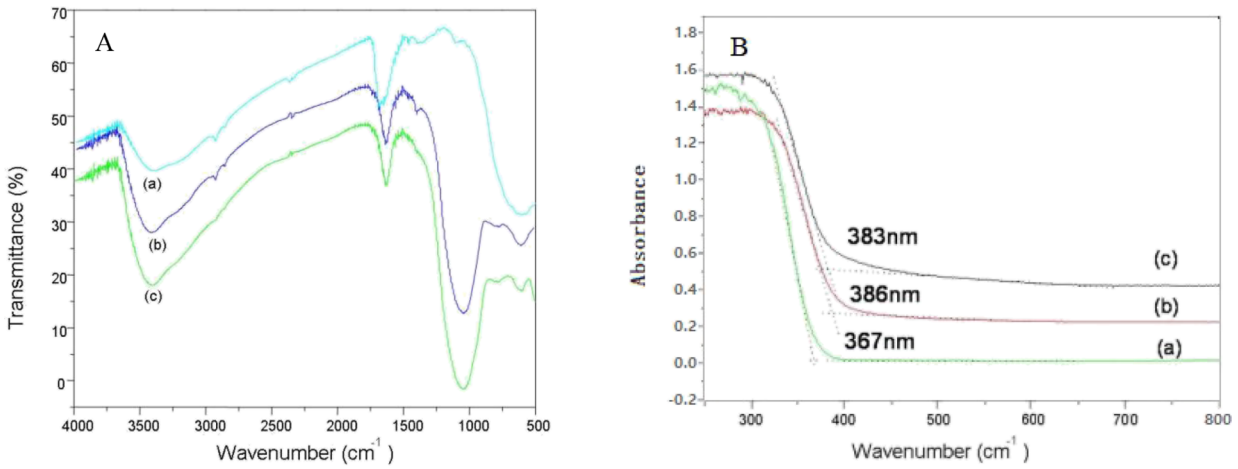

Figure 4. (A) FTIR and (B) UV−vis spectra of TiO_2 (a), N-TiP (b), and TiP (c)

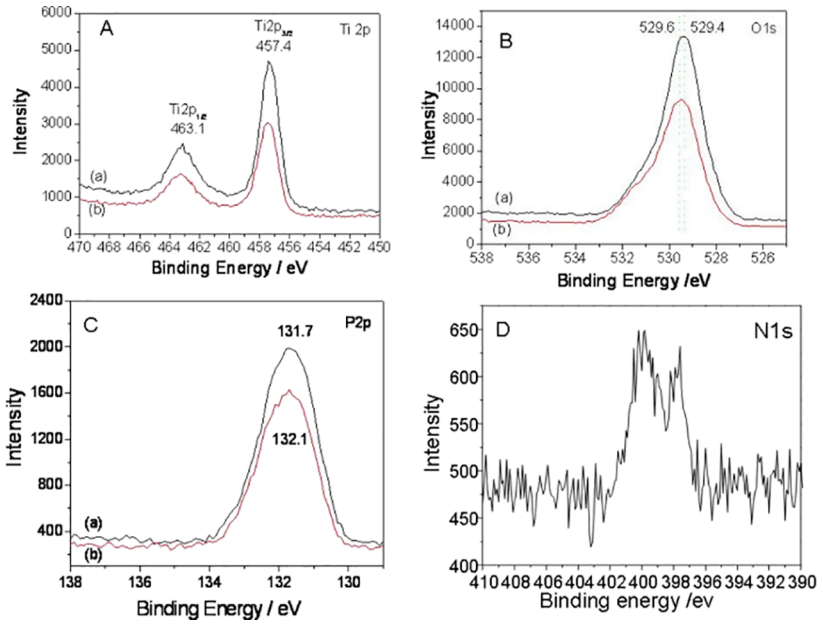

Figure 5. High-resolution XPS spectra of (A) the Ti 2p and (B) O 1s and (C) P 2p regions taken on the surface of TiP (a) and N-TiP (b). The N 1s XPS spectra of N-TiP (D).

surface-adsorbed water and hydroxyl groups. The strong spectra in the region between 1000 and 1050 cm^{-1} centered at 1030 cm^{-1} result from Ti−O−P skeletal stretching vibrations of TiP and N-TiP samples[34] but is absent in the pure TiO_2. The small bands at 1400 cm^{-1}, observed in the spectra of the nitridation samples N-TiP, are attributed to the nitrogen atoms embedded in the TiO_2 network,[37] which are not found in the samples TiO_2 and TiP. Small peaks in the range of 500−790 cm^{-1} are formed by the vibration of the Ti−O bond. On the whole, the FTIR data support that phosphorus and nitrogen are incorporated into the framework in the form of Ti−O−P, O−Ti−N, and/or O−P−N bonds.[38,39] Furthermore, UV−vis diffuse reflectance spectroscopy was performed to assess the optical properties and electronic structure of the synthesized samples (Figure 4B).

The absorption at 367 nm is for the pure TiO_2, while the TiP and N-TiP are at 386 and 383 nm, reflecting a noticeable shift of the absorption onset to the visible-light region. Meanwhile, the band gap (E_g) can be calculated by the formula E_g (eV) = 1240/λ_g(nm), where λ_g stands for the wavelength value corresponding to the intersection point of the vertical and horizontal parts of the spectra. The band gap (E_g) of the TiO_2, N-TiP, and TiP is estimated to be 3.38, 3.20, and 3.24 eV, respectively. Hence, such a band gap shortening could be the result of phosphorus and nitrogen into the titania framework.

In order to investigate the nitrogen states as well as surface nitrogen content of the nitrogen-doped material, high-resolution XPS measurement on the sample N-TiP is carried on, indicating that the presence of nitrogen was not only at the surface but also was incorporated into the sublayers of the N-doped sample. As described in the literature,[31,32] N and P atoms are probably incorporated as anions and cations, replacing O and Ti ions, respectively. This can be further confirmed by the comparison of the Ti 2p and the O 1s XPS spectra. When scanning the Ti 2p XPS regions (Figure 5a,b), the peak appears at 457.4 and 464.1 eV, which are notably lower than the binding energy of Ti^{4+} in TiO_2 (459 eV for Ti $2p_{3/2}$ and 464.8 for Ti $2p_{1/2}$). As discussed by others,[40,41] a shift toward lower binding energy upon nitrogen treatment

https://doi.org/10.1021/acsomega.3c07222
ACS Omega 2023, 8, 49129−49136

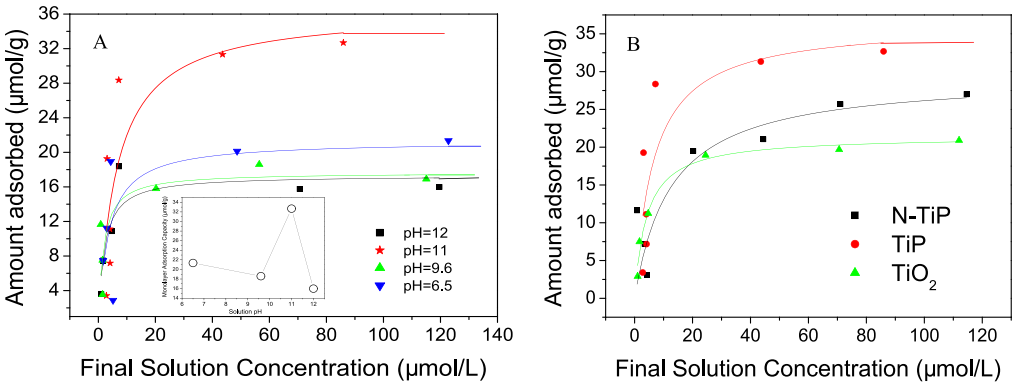

Figure 6. (A) Adsorption isotherms of lysozymes on TiP at various pH values and (inset) the maximum amount adsorbed of Lz on TiP at the various pH values; (B) adsorption isotherms of TiO_2, TiP, and N-TiP for proteins at pH = 11.

displays the successful incorporation of nitrogen into the TiO_2 lattice. After doping (when the N atom replaces the O atom out of the lattice), the valence state of the Ti cation can be reduced. The binding energy of the Ti $2p_{3/2}$ peak shifts to lower energies when the valence state of Ti^{4+} is reduced to Ti^{3+} and Ti^{2+}. Thus, the observed Ti $2p_{3/2}$ binding energy of N-TiP can be attributed to the formation of Ti−O−P and O−Ti−N bonding by partially substituting the O atom in the TiO_2 lattice with an N atom. This shifts the binding energies of the Ti 2p electrons to an observed lower value. The XPS spectra of the O 1s region (Figure 5b) show the main peak at 529.4 eV for TiP, attributed to the oxygen atoms of TiO_2 and the O in Ti−O−P, respectively, corresponding to the literature.[31]

To get further evidence, the P states were collected in Figure 5c and the P 2p XPS spectra of N-TiP with a marked peak at 131.7 eV, which suggests that phosphor in the sample exists in a pentavalent-oxidation state (P^{5+}).[42] In addition, it is important to note that no peaks are found around 128.6 eV, which is consistent with the Ti−P bond when P atoms replace O atoms in the TiO_2 crystalline lattice,[43] in other words, phosphorus atoms have entered into the lattice of TiO_2. A similar state can be observed in sample N-TiP, indicating that the possibility of clarifying the effect of N-modification is still unclear.

The states of nitrogen in sample N-TiP were further analyzed by XPS. As shown in Figure 5d, the sample shows the peak at 397 and 399 eV, which can be attributed to atomic nitrogen and the formation of O−Ti−N bonds.[44] However, to understand the broad peak in the 396−403 eV region,[45] some researchers[46,47] attributed the N 1s peaks with binding energies of 400 and 402 eV to molecularly adsorbed nitrogen species. Chen and Burda[48] observed an N 1s core level at 401.3 eV in nitrogen-doped titania nanoparticles and suggested that it is attributed to the N atoms in the environment of O−Ti−N. According to the literature,[46−49] the observed N 1s core level peak at 399 eV was attributed to the O−Ti−N linkage in the crystalline TiO_2 lattice. This can be further confirmed by the shifted binding energy of the Ti 2p and O 1s.[49]

3.2. Adsorption of Lysozymes. Lysozyme is an antimicrobial and spherical protein with two characteristic cross sections: a side of dimensions of roughly 3.0 × 4.5 nm^2 and an end of dimensions 3.0 × 3.0 nm^2.[50] Its molecular mass is 14,400 Da. The isoelectric point of Lz is as high as 10.8[51] because it contains numerous amino acid residues.

Figure 6A represents the adsorption isotherms of Lz adsorbed on TiP, N-TiP, and TiO_2 at a solution pH of 11. The correlation textural parameters and monolayer adsorption capacities are shown in Table 1. It can be seen from Table 1 that the adsorption ability decreases in the following order: TiP > N-TiP > TiO_2. The maximal adsorption capacity of TiP is 32.68 μmol/g (470 mg/g) and 26 μmol/g (374 mg/g) was observed for N-TiP, whereas TiO_2 is 20.9 μmol/g (301 mg/g). Comparing with the high surface areas of samples, such as SBA-15 (S_{BET} = 910m^2/g vs q_e = 508 mg/g), MCM-41 (S_{BET} = 1135 m^2/g vs q_e = 405 mg/g), and carbon materials (S_{BET} = 1600 m^2/g vs q_e = 390 mg/g), the adsorption-efficiency of TiP is rather higher than those reference report.[23] The high specific surface area is particularly important for lysozyme adsorption on the surface of mesoporous materials because lysozyme adsorption is monolayer adsorption. Among these synthetic materials, TiP shows the strongest adsorption ability due to the maximum specific surface area and pore volume, which cause lysozyme to have numerous adsorption centers. N-TiP possesses the largest aperture, which is convenient for lysozyme molecules to enter the pore and spread out to cover the whole surface of the pore. Therefore, the material properties dominate the adsorption capability of Lz.

During the range of physiological temperature, no detectable change in the structure was observed within the pH range from 1.5 to 12. The adsorption isotherms of lysozyme on TiP at different buffer solutions with pH from 6.5 to 12 are shown in Figure 6. The adsorption was tested at pH = 6.5, 9.6, 11, and 12. These isotherms are monolayer adsorption and show a sharp initial rise, suggesting a high affinity between lysozyme and the adsorbent surface. Then the adsorption amount increases slowly and eventually, an adsorption plateau appears in a higher equilibrium concentration. The isotherms are in accordance with typical Langmuir monolayer adsorption isotherms. The Langmuir model is employed by the solid line in this figure that is expected a fit of experimental data. The monolayer adsorption capacity is calculated by using the Langmuir equation.

$$n_s = Kn_m c/(1 + Kc)$$

where K is the Langmuir constant, c is the lysozyme concentration, n_m is the monolayer adsorption capacity, and n_s is the amount of Lz adsorbed on the adsorbent.

The maximal adsorption was carried out at pH = 11, which is the isoelectric point (pI, the pH value in solution at which the sum of the charges on the protein is zero) of Lz.[51] It is well-known that the protein is positively charged at a pH below pI and negatively charged at a pH above pI. Meanwhile, the

https://doi.org/10.1021/acsomega.3c07222
ACS Omega 2023, 8, 49129−49136

amount of adsorption changes with the pH of the solution. The maximum adsorption of Lz amounts to 32.68 μmol/g (470 mg/g) at a pH of 11, while only 15.99 μmol/g are adsorbed at pH = 12. The monolayer adsorption capacity at pH = 11 is almost twice the amount of the Lz adsorbed at pH = 12 (Figure 6B inset). Both the electrostatic interactions and the hydrophobic interactions are important forces in the way of the adsorption of lysozymes. With a decrease in pH from 11 to 6.5, the net positive charges of lysozyme molecules start to increase. The increased lateral repulsion on lysozyme monolayer leads to the enlargement of Lz molecules and further occupation of more space than in a solution with a pH near the pI. Thus, the electrostatic attraction between Lz and the adsorbent is decreased. The monolayer capacity at a pH below pI is lower than in a solution with a pH near the PI. Moreover, near the isoelectric point, the net charge of the Lz is low, and the lateral repulsion between the Lz molecules is minimal. In addition, hydrophobic interactions are more dominant near the pI than electrostatic interactions. Therefore, the monolayer capacity is the maximum at a pH near the pI. When the solution pH is 12, the surface of the lysozyme molecule becomes negatively charged, which enhances the electrostatic repulsion between protein molecules. Therefore, the amount adsorbed decreases in the same way. It also has been reported earlier[52] that lysozyme hardly adsorbs under the conditions of electrostatic repulsion at hydrophobic surfaces, which is in line with our findings. From the above analysis, we believe that the hydrophobic interactions are more important than the electrostatic interactions at pI, while the solution pH value varies both below and above pI, Coulombic forces become the more dominant driving force for the adsorption of protein onto the adsorbents.

4. CONCLUSIONS

In this study, the nonmetallic elements phosphorus-doped titanium oxide (TiP) and phosphorus−nitrogen codoped mesoporous titanium oxide (N-TiP) were prepared by a one-step hydrothermal method in an ethanol system at room temperature. Using inorganic phosphoric acid as a phosphorus source, phosphorus-modified mesoporous titanium oxide was synthesized by controlling the hydrolysis of tetrabutyl titanate and the process of nanoparticle aggregation and self-assembly without any surfactant. The synthesis method is simple and template-free, producing uniform aggregated nanoparticles with the amorphous phase. Furthermore, the adsorption of lysozyme onto the resultant material was observed and the results show that mesoporous titanium oxides are predominantly anatase, TiP and N-TiP are amorphous but the former's specific surface area is bigger, reaching about 317 m^2/g. Partial Ti of Ti−O−Ti bonds in mesoporous titanium oxide is replaced by phosphorus, and the Ti−O−P new bond is generated. O−Ti−N bond is generated by doping nitrogen in the form of negative ions. The adsorption performance of doping or modified mesoporous titanium oxide materials for lysozymes is greatly increased. The results denoted Lz adsorption correspond to the monolayer adsorption and to the type of Langmuir isotherm. At the isoelectric point, that is, at pH = 11, the adsorption capacity of TiP to lysozyme is the highest, which is 32.68 μmol/g. TiP has the largest specific surface area and pore volume, which allows more adsorption centers for lysozyme; i.e., TiP has a stronger adsorption capacity. For N-TiP, it has the largest pore size, which facilitates the lysozyme molecules to enter into the pore channels and disperse in them, thus covering all surfaces. However, since lysozyme adsorption is monolayer adsorption, a large specific surface area is more important for lysozyme adsorption. TiP has a larger specific surface area and pore volume than N-TiP and TiO_2, so it has the strongest adsorption capacity.

AUTHOR INFORMATION

Corresponding Authors

Yajing Wang − *School of Gemology and Materials, Hebei GEO University, Shijiazhuang 050031, China; Engineering Research Center for Silicate Solid Waste Resource Utilization of Hebei Province, Shijiazhuang 050031, China; Hebei Key Laboratory of Green Development of Rock Mineral Materials, Shijiazhuang 050031, China*; Email: wyjbs@hgu.edu.cn

Tiezhen Ren − *College of Chemical Engineering, Xinjiang University, Urumqi, Xinjiang 830046, China*; Email: rtz@xju.edu.cn

Authors

Xu Zhang − *School of Gemology and Materials, Hebei GEO University, Shijiazhuang 050031, China; Engineering Research Center for Silicate Solid Waste Resource Utilization of Hebei Province, Shijiazhuang 050031, China; Hebei Key Laboratory of Green Development of Rock Mineral Materials, Shijiazhuang 050031, China*

Peng Liu − *School of Gemology and Materials, Hebei GEO University, Shijiazhuang 050031, China; Engineering Research Center for Silicate Solid Waste Resource Utilization of Hebei Province, Shijiazhuang 050031, China; Hebei Key Laboratory of Green Development of Rock Mineral Materials, Shijiazhuang 050031, China*; orcid.org/0000-0002-8728-1209

Zhao Liu − *School of Water Resources and Environment, Hebei GEO University, Shijiazhuang 050031, China*

Ziqian Wang − *School of Gemology and Materials, Hebei GEO University, Shijiazhuang 050031, China*

Complete contact information is available at: https://pubs.acs.org/10.1021/acsomega.3c07222

Notes

The authors declare no competing financial interest.

ACKNOWLEDGMENTS

This research was funded by the Key R&D Project from the Science and Technology Department of Tibet (award number XZ202101ZY0008G) and National College Students Innovation and Entrepreneurship Training Project (award number 202310077020).

REFERENCES

(1) Mostafa, N. G.; Yunnus, A. F.; Elawwad, A. Adsorption of Pb(II)from water onto ZnO, TiO_2, and Al_2O_3:Process study, adsorption behaviour, and thermodynamics. *Adsorption Science & Technology* **2022**, *2022*, 1−13.

(2) Rehman, M. U.; Rehman, W.; Waseem, M.; Hussain, S.; Haq, S.; Rehman, A. U. Adsorption mechanism of Pb^{2+} ions by Fe_3O_4, SnO_2, and TiO_2 nanoparticles. *Environ. Sci. Pollut. Res.* **2019**, *26*, 19968−19981.

(3) Li, W.; Zhangxiong, W.; Wang, J.; Elzatahry, A. A.; Zhao, D. A Perspective on Mesoporous TiO_2 Materials. *Chem. Mater.* **2014**, *26*, 287−298.

(4) Abbas, M. Potential of Titanium Dioxide to Remove Bromothymol Blue (BTB) in Aqueous Solution by Batch Mode

https://doi.org/10.1021/acsomega.3c07222
ACS Omega 2023, 8, 49129−49136

Adsorption−Kinetic, Isotherm and Thermodynamic Studies. *Fibers Polym.* **2023**, *24* (2), 603−612.
(5) Chen, R.; Yan, L.; Lin, L.; Deng, C.; Zhang, Z. Coadsorption of CO and CH_4 on the Au doped SnO_2 (110) surface: a first principles investigation. *Phys. Scr.* **2022**, *97* (4), No. 045403.
(6) Bazargan, G.; Schweigert, I. V.; Gunlycke, D. Adsorption of organophosphate nerve agent vx on the (101) surface of anatase titanium dioxide. *Surf. Sci.* **2022**, *716*, No. 121957.
(7) Bożena, G.; Zakrzewska, D.; Szymczycha, B. Sorption of Cr, Pb,Cu,Zn,Cd,Ni, and Co to nano-TiO_2 in seawater. *Water Sci. Technol.* **2018**, *77* (1), 145−158.
(8) Wang, D. X.; Wang, P. F.; Wang, D.; Wang, P. F.; Wang, C.; Ao, Y. Effects of interactions between humic acid and heavy metal ions on the aggregation of TiO_2 nanoparticles in water environment. *Environ. Pollut.* **2019**, *248*, 834−844.
(9) Chen, B.; Li, L.; Liu, L.; Cao, J. Molecular simulation of adsorption properties of thiol-functionalized titanium dioxide (TiO_2) nanostructure for heavy metal ions removal from aqueous solution. *J. Mol. Liq.* **2022**, *346*, No. 118281.
(10) Han, D. S.; Batchelor, B.; Park, S. H.; Abdel-Wahab, A. As(V) adsorption onto nanoporous titania adsorbents (NTAs): Effects of solution composition. *J. Hazard. Mater.* **2012**, *229*−*230*, 273−281.
(11) Belessi, V.; Romanos, G.; Boukos, N.; Lambropoulou, D.; Trapalis, C. Removal of Reactive Red 195 from aqueous solutions by adsorption on the surface of TiO_2 nanoparticles. *J. Hazard. Mater.* **2009**, *170* (2−3), 836−844.
(12) Hallam, L.; Papasergio, A.; Lessio, M.; Veliscek-Carolan, J. Phosphate functionalised titania for heavy metal removal from acidic sulfate solutions. *J. Colloid Interface Sci.* **2021**, *600*, 719−728.
(13) Feng, S. B.; Zhao, C. X.; Long, X.; Zhou, J.; Chen, W. Synthesis and photo-degradation properties of C-doping mesoporous titanium dioxide. *Acta Pet. Sin.* **2009**, *25*, 32−36.
(14) Ren, J.; Zheng, L.; Yang, F.; Meng, P. Electron-scale insights into the single and coadsorption Cd(II)behaviors of a metal-nonmetal-modified titanium dioxide. *Adsorp. Sci. Technol.* **2021**, *2021*, No. 4556493.
(15) Peng, W.; Du, S.; Shaoning, Z.; Xieyi, H.; Fuqiang, H. Constructing mesoporous phosphated titanium oxide for efficient Cr(III) removal. *J. Hazard. Mater.* **2019**, *384* (165), No. 121278.
(16) Zhang, W. L.; Yan, Y.; et al. Preparation and adsorption property of Br-doped nano porous TiO_2. *Chinese J. Nonferr. Met.* **2012**, *12*, 3439−3445.
(17) Ren, J.; Zheng, L.; et al. Competitive adsorption of Cd(II), Pb(II) and Cu(II) ions from acid mine drainage with zero-valent iron/phosphoric titanium dioxide:XPS qualitative analyses and DFT quantitative calculations. *Chemical Engineering Journal* **2022**, *445*, No. 136778.
(18) Xiong, L.; Wang, Y.; Cui, W.; Chen, L.; Luo, Q.; Cao, X.; Liu, Y. H. Preparation of ion-doped amorphous titanium phosphates and their adsorption properties for U(VI). *Journal of Radioanalytical and Nuclear Chemistry* **2023**, *332* (4), 1303−1314.
(19) Maeda, H.; Kato, K.; Kasuga, T. Adsorption behavior of proteins on calcium silicate hydrate in Tris and phosphate buffer solutions. *Mater. Lett.* **2016**, *167* (15), 112−114.
(20) Chang, Y. K.; Cheng, H. I.; Ooi, C. W.; Song, C. P.; Liu, B. L. Adsorption and purification performance of lysozyme from chicken egg white using ion exchange nanofiber membrane modified by ethylene diamine and bromoacetic acid. *Food Chem.* **2021**, *358* (1), No. 129914.
(21) Liu, B. L.; Ooi, C. W.; Ng, I. S.; Show, P. L.; Chang, Y. K. Effective purification of lysozyme from chicken egg white by tris(hydroxymethyl) aminomethane affinity nanofiber membrane. *Food Chem.* **2020**, *327* (1), No. 127038.
(22) Cao, Y. D.; Dang, L. Q.; Bai, D.; Lei, Z. B.; Liu, M. Y. Adsorption of Lysozymes on Fe/CMK-5 Composites Synthesized by Chemical Vapor Deposition. *Acta Phys. Chim. Sin.* **2010**, *26* (6), 1593−1598.
(23) Vinu, A.; Miyahara, M.; Ariga, K. Biomaterial immobilization in nanoporous carbon molecular sieves: influence of solution pH, pore volume, and pore diameter. *J. Phys. Chem. B* **2005**, *109* (13), 6436−6441.
(24) Ma, T. Y.; Zhang, X. J.; Yuan, Z. Y. Hierarchical Meso-/Macroporous Aluminum Phosphonate Hybrid Materials as Multifunctional Adsorbents. *J. Phys. Chem. C* **2009**, *113* (29), 12854−12862.
(25) Li, H.; Wei, X.; Yang, J.; Zhang, R.; Yang, J. The bacteriolytic mechanism of an invertebrate-type lysozyme from mollusk Octopus ocellatus. *Fish Shellfish. Immunol.* **2019**, *93*, 232−239.
(26) Park, K. H.; Mondal, S.; Ghosh, S.; Das, S.; Bhaumik, A. Enhanced efficiency in dye-sensitized solar cells based on mesoporous titanium phosphate photoanode. *Microporous Mesoporous Mater.* **2016**, *225*, 255 DOI: 10.1016/j.micromeso.2015.11.059.
(27) Guo, S. Y.; Han, S.; Chi, B.; Pu, J.; Li, J. Synthesis of shape-controlled mesoporous titanium phosphate nanocrystals: The hexagonal titanium phosphate with enhanced hydrogen generation from water splitting. *Int. J. Hydrogen Energy* **2014**, *39* (6), 2446−2453.
(28) Wang, X. Y.; Yang, X. L.; Cai, J. H.; Miao, T. T.; Li, L. H.; Li, G.; Wang, C. Novel flower-like titanium phosphate microstructures and their application in lead ion removal from drinking water. *J. Mater. Chem. A* **2014**, *2* (19), 6718−6722.
(29) Wang, Y.; Zeng, D.; Dai, Y.; Fang, C.; Liu, Y. The Adsorptive Ability of 3D Flower-Like Titanium Phosphate for U(VI) in Aqueous Solution. *Water Air Soil Pollut.* **2020**, *231* (9), 464 DOI: 10.1007/s11270-020-04817-2.
(30) Kapoor, M. P.; Inagaki, S.; Yoshida, H. Novel zirconium-titanium phosphates mesoporous materials for hydrogen production by photoinduced water splitting. *J. Phys. Chem. B* **2005**, *109* (19), 9231−9238.
(31) Yu, J. C.; Zhang, L.; Zheng, Z.; Zhao, J. Synthesis and Characterization of Phosphated Mesoporous Titanium Dioxide with High Photocatalytic Activity. *Chem. Mater.* **2003**, *15* (11), 2280−2286.
(32) Ahmad, N.; Mahmood, T. Preparation and properties of 4-aminobenzoic acid-modified polyvinyl chloride/titanium dioxide and PVC/TiO_2 based nanocomposites membranes. *Polymers Polym. Compos.* **2022**, *30*, No. 09673911221099301, DOI: 10.1177/09673911221099301.
(33) Fan, X.; Yu, T.; Wang, Y.; Zheng, J.; Gao, L.; Li, Z.; Ye, J.; Zou, Z. Role of phosphorus in synthesis of phosphated mesoporous TiO_2, photocatalytic materials by EISA method. *Appl. Surf. Sci.* **2008**, *254* (16), 5191−5198.
(34) Han, S.; Sun, J. B.; Guo, S. Y.; Jiang, L.; He, D. P. Phosphorus Doped Titania Materials: Synthesis, Characterization and Visible-Light Photocatalytic Activity. *Advanced Materials Research* **2011**, *183*−*185*, 2059−2062.
(35) Tang, M. L.; Chen, J.; Wang, P. F.; Wang, C.; Ao, Y. H.; Yanhui, A. Highly efficient adsorption of uranium(VI) from aqueous solution by a novel adsorbent: titanium phosphate nanotubes. *Environ. Sci. Nano* **2018**, *5* (10), 2304−2314.
(36) Sarkar, K.; Nandi, M.; Bhaumik, A. Enhancement in microporosity and catalytic activity on grafting silica and organosilica moieties in lamellar titanium phosphate framework. *Applied Catalysis A General* **2008**, *343* (1), 55−61.
(37) Burda, C.; Lou, Y.; Chen, X.; Anna, C.S.S.; Stout, J.; James, L.G. Enhanced Nitrogen Doping in TiO_2 Nanoparticles. *Nano Lett.* **2003**, *3* (8), 1049−1051.
(38) Li, H.; Li, J.; Huo, Y. Highly Active TiO_2N Photocatalysts Prepared by Treating TiO_2 Precursors in NH_3/Ethanol Fluid under Supercritical Conditions. *J. Phys. Chem. B* **2006**, *110* (4), 1559−1565.
(39) Wang, Q.; Zhong, L.; Sun, J.; Shen, J. A Facile Layer-by-Layer Adsorption and Reaction Method to the Preparation of Titanium Phosphate Ultrathin Films. *Chem. Mater.* **2005**, *17* (13), 3563−3569.
(40) Ren, T. Z.; Yuan, Z. Y.; Azioune, A.; Pireaux, J. J.; Su, B. L. Tailoring the Porous Hierarchy of Titanium Phosphates. *Langmuir* **2006**, *22* (8), 3886−3894.
(41) Du, X.; Wang, Y.; Mu, Y.; Gui, L.; Wng, P.; Tang, Y. A New Highly Selective H_2 Sensor Based on TiO_2/PtO−Pt Dual-Layer Films. *Chem. Mater.* **2002**, *14*, 3953−3957.

https://doi.org/10.1021/acsomega.3c07222
ACS Omega 2023, 8, 49129−49136

(42) Splinter, S. J.; Rofagha, R.; Mcintyre, N. S.; Erb, U. XPS Characterization of the Corrosion Films Formed on Nanocrystalline Ni−P Alloys in Sulphuric Acid. *Surf. Interface Anal.* **1996**, *24* (3), 181−186.
(43) Baunack, S.; Oswald, S.; Scharnweber, D. Depth distribution and bonding states of phosphorus implanted in titanium investigated by AES, XPS and SIMS. *Surf. Interface Anal.* **1998**, *26* (6), 471−479.
(44) Lin, L.; Zheng, R. Y.; Xie, J. L.; Zhu, Y. X.; Xie, Y. C. Synthesis and characterization of phosphor and nitrogen co-doped titania. *Applied Catalysis B Environmental* **2007**, *76* (1−2), 196−202.
(45) Himpsel, F. J.; Mcchesney, J. L.; Crain, J. N.; Kirakosian, A.; Petrovykh, D. Y. Stepped Silicon Surfaces as Templates for One-Dimensional Nanostructures. *J. Phys. Chem. B* **2004**, *108* (38), 14484−14490.
(46) Sakthivel, S.; Janczarek, M.; Kisch, H. Visible Light Activity and Photoelectrochemical Properties of Nitrogen-Doped TiO_2. *journal of physical chemistry, B. Condensed matter, materials, surfaces, interfaces & biophysical* **2004**, *108* (50), 19384−19387.
(47) Delfino, M.; Fair, J. A.; Hodul, D. X-ray photoemission spectra of reactively sputtered TiN. *J. Appl. Phys.* **1992**, *71* (12), 6079−6085.
(48) Chen, X.; Burda, C. Photoelectron Spectroscopic Investigation of Nitrogen-Doped Titania Nanoparticles. *J. Phys. Chem. B* **2004**, *108*, 15446−15449.
(49) Gao, B.; Ma, Y.; Cao, Y.; Yang, W.; Yao, J. Great enhancement of photocatalytic activity of nitrogen-doped titania by coupling with tungsten oxide. *J. Phys. Chem. B* **2006**, *110* (29), 14391−14397.
(50) Kharakoz, D. P.; Sarvazyan, A. P. Hydrational and intrinsic compressibilities of globular proteins. *Biopolymers* **1993**, *33*, 11−14.
(51) Wilson, K. P.; Malcolm, B. A.; Matthews, B. W. Structural and thermodynamic analysis of compensating mutations within the core of chicken egg white lysozyme. *J. Biol. Chem.* **1992**, *267* (15), 10842−10849.
(52) Ball, V.; Ramsden, J. J. Absence of Surface Exclusion in the First Stage of Lysozyme Adsorption Is Driven through Electrostatic Self-Assembly. *J. Phys. Chem. B* **1997**, *101* (28), 5465−5469.

https://doi.org/10.1021/acsomega.3c07222
ACS Omega 2023, 8, 49129−49136